Acta Biomaterialia 86 (2019) 125–134

Contents lists available at ScienceDirect

Acta Biomaterialia

journal homepage: www.elsevier.com/locate/actabiomat

Full length article

Biophysical phenotypes and determinants of anterior *vs.* posterior primitive streak cells derived from human pluripotent stem cells

Feng Lin [a,b], Yue Shao [b], Xufeng Xue [b], Yi Zheng [b], Zida Li [b], Chunyang Xiong [a,c,*], Jianping Fu [b,d,e,*]

[a] Department of Mechanics and Engineering Science, College of Engineering, Peking University, Beijing 100871, China
[b] Department of Mechanical Engineering, University of Michigan, Ann Arbor, MI 48109, USA
[c] Academy for Advanced Interdisciplinary Studies, Peking University, Beijing 100871, China
[d] Department of Biomedical Engineering, University of Michigan, Ann Arbor, MI 48109, USA
[e] Department of Cell and Developmental Biology, University of Michigan Medical School, Ann Arbor, MI 48109, USA

ARTICLE INFO

Article history:
Received 26 July 2018
Received in revised form 7 January 2019
Accepted 10 January 2019
Available online 11 January 2019

Keywords:
Primitive streak
Biophysical phenotypes
Cell mechanics
Human pluripotent stem cells

ABSTRACT

Formation of the primitive streak (PS) marks one of the most important developmental milestones in embryonic development. However, our understanding of cellular mechanism(s) underlying cell fate diversification along the anterior-posterior axis of the PS remains incomplete. Furthermore, differences in biophysical phenotypes between anterior and posterior PS cells, which could affect their functions and regulate their fate decisions, remain uncharacterized. Herein, anterior and posterior PS cells were derived using human pluripotent stem cell (hPSC)-based *in vitro* culture systems. We observed that anterior and posterior PS cells displayed significantly different biophysical phenotypes, including cell morphology, migration, and traction force generation, which was further regulated by different levels of Activin A- and BMP4-mediated developmental signaling. Our data further suggested that intracellular cytoskeletal contraction could mediate anterior and posterior PS differentiation and phenotypic bifurcation through its effect on Activin A- and BMP4-mediated intracellular signaling events. Together, our data provide new information about biophysical phenotypes of anterior and posterior PS cells and reveal an important role of intracellular cytoskeletal contractility in regulating anterior and posterior PS differentiation of hPSCs.

Statement of Significance

Formation of the primitive streak (PS) marks one of the most important developmental milestones in embryonic development. However, molecular and cellular mechanism(s) underlying functional diversification of embryonic cells along the anterior-posterior axis of the PS remains incompletely understood. This work describes the first study to characterize the biophysical properties of anterior and posterior PS cells derived from human pluripotent stem cells (hPSCs). Importantly, our data showing the important role of cytoskeleton contraction in controlling anterior *vs.* posterior PS cell phenotypic switch (through its effect on intracellular Smad signaling activities downstream of Activin A and BMP4) should shed new light on biomechanical regulations of the development and anterior-posterior patterning of the PS. Our work will contribute significantly to uncovering new biophysical principles and cellular mechanisms driving cell lineage diversification and patterning during the PS formation.

1. Introduction

One of the most important challenges in studying embryonic development is to understand cellular behaviors and molecular mechanisms underlying the large-scale tissue morphogenesis and patterning that arise during gastrulation [1]. Gastrulation is a critical developmental stage of the early embryonic development, involving patterning of mesodermal and endodermal precursors

* Corresponding authors at: Department of Mechanics and Engineering Science, College of Engineering, Peking University, Beijing 100871, China (C. Xiong); Department of Mechanical Engineering, University of Michigan, Ann Arbor, MI 48109, USA (J. Fu).
E-mail addresses: cyxiong@pku.edu.cn (C. Xiong), jpfu@umich.edu (J. Fu).

https://doi.org/10.1016/j.actbio.2019.01.017
1742-7061/

and their migration into the embryo through a structure known as the primitive streak (PS) [2,3]. The PS serves as a conduit of cell migration for the formation and organization of the three germ layers during gastrulation [4]. Although migration patterns of mesodermal and endodermal precursors through the PS have been studied in great details [4], molecular mechanism(s) underlying the development of the PS and functional diversification of embryonic cells along the anterior-posterior axis of the PS remain incompletely understood. Human pluripotent stem cells (hPSCs), which reside in a developmental state similar to the pluripotent epiblast, offer unprecedented opportunities to study human development *in vitro* and to develop new sources of human cells, including anterior and posterior PS cells [5,6]. In this work, we sought to examine specifically biophysical phenotypes of anterior and posterior PS cells derived from hPSCs and how cellular biophysical properties could in turn regulate anterior and posterior PS differentiation of hPSCs.

The PS structure is composed mainly of mesoderm precursors that are *en route* of the epithelial-to-mesenchymal transition (EMT) process to become cells with mesenchymal phenotypes [7]. Development of the PS structure and its patterning along the anterior-posterior axis are regulated by graded developmental signaling mediated by soluble factors such as fibroblast growth factors (FGFs), NODAL/Activin A, bone morphogenetic proteins (BMPs), and WNT-related molecules [6,8]. These well-described anterior-posterior morphogen gradients are thought to pattern mesoderm subtypes [9–11], such as specifying anterior mesodermal fates like cardiomyocytes versus posterior mesodermal fates like blood. Mechanistically, the transforming growth factor beta (TGF-β) signaling family members such as Activin A and BMP4 work synergistically to activate downstream signaling pathways to drive PS formation and patterning.

Tissue morphogenesis and patterning, including the development and anterior-posterior patterning of the PS, are controlled not only by biochemical cues from the local cell microenvironment but also by co-existing biophysical cues that together drive and shape tissue development and formation [12–14]. During embryonic development, embryonic cells undergo dynamic changes in cell shape and cytoskeletal organization, which in turn affect mechanical inputs of tissue morphogenesis via changes in cell mechanical properties such as cell migratory behaviors and traction force generation [12,15,16]. As an example, during *Drosophila* axis elongation, cell intercalation is driven by polarized actomyosin contractility, which promotes disassembly of cell-cell interfaces separating anterior and posterior cell neighbors [17], supporting that biophysical properties of anterior and posterior PS cells play prominent roles in subsequent patterning into specific tissue subtypes. In this work, we thus sought to examine specifically biophysical properties of anterior and posterior PS cells and further determine how cellular biophysical properties could in turn regulate anterior and posterior PS differentiation of hPSCs (H9 hESC line). Our study provides new understanding of biomechanical regulation of the development and anterior-posterior patterning of the PS, contributing to uncovering biophysical principles and cellular mechanisms driving cell lineage diversification and patterning during the PS formation.

2. Results

2.1. Differentiation of anterior and posterior primitive streak cells

Anterior PS (AntPS)-like cells were derived from hPSCs (H9 hESC line) by treating hPSCs with fibroblast growth factor 2 (FGF2), LY294002 (phosphatidylinositol 3-kinase inhibitor), bone morphology protein 4 (BMP4), and Activin A (Fig. 1A; see Materials and Methods) [6,18]. To derive posterior PS (PostPS) cells from hPSCs (H9 hESC line), Activin A was removed from differentiation

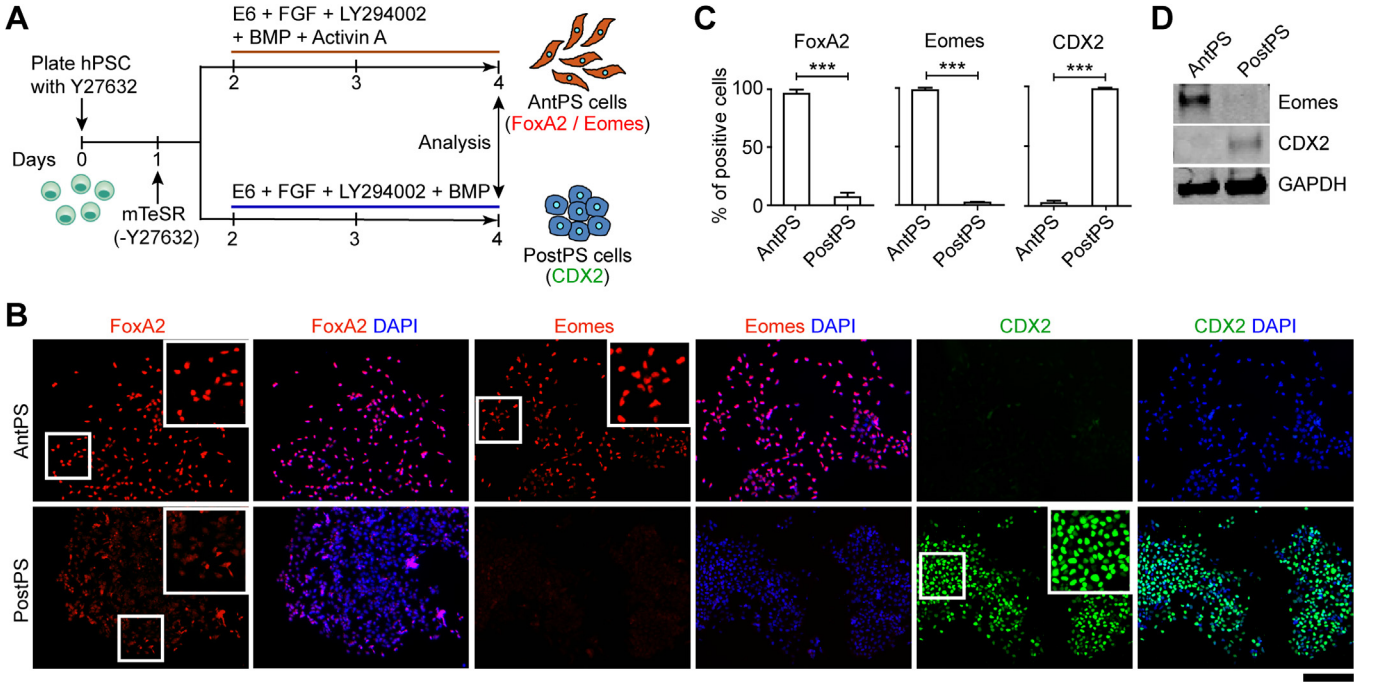

Fig. 1. Derivation of anterior primitive streak (AntPS) cells and posterior primitive streak (PostPS) cells from hPSCs. (A) Schematic diagram showing experimental design for differentiating hPSCs into AntPS and PostPS cells, respectively. (B) Representative immunofluorescence images showing staining for FoxA2, Eomes, and CDX2 in AntPS and PostPS cells. Square inserts highlight nuclear staining of respective lineage markers as indicated. Scale bar, 200 μm. (C) Bar plots showing percentages of cells with dominant nuclear staining for FoxA2, Eomes, and CDX2 under indicated conditions. Data represent the mean ± SD calculated from at least 10 random fields in one experiment that is representative of three independent experiments. *P* values were calculated using one-way ANOVA followed by *t*-test analysis. ***, $P < 0.001$. (D) Western blotting showing expression levels of Eomes and CDX2 in AntPS and PostPS cells derived from hPSCs.

medium. After 48 h of differentiation, cells were stained for AntPS cell markers FoxA2 and Eomes and PostPS cell marker CDX2 (Fig. 1B). With Activin A supplemented in differentiation medium, 96 ± 3.6% and 98 ± 1.3% of cells were FoxA2$^+$ and Eomes$^+$, respectively, whereas only 2.5 ± 1.7% of cells were CDX2$^+$ (Fig. 1B&C), supporting efficient AntPS cell differentiation from hPSCs and a pure AntPS cell population. In distinct contrast, without Activin A supplemented in differentiation medium, 98 ± 1% of cells were CDX2$^+$, whereas only 7 ± 3.8% and 2 ± 0.8% of cells were FoxA2$^+$ and Eomes$^+$, respectively (Fig. 1B&C), suggesting a pure PostPS cell population. Western blotting further confirmed upregulated protein expression levels of Eomes and CDX2 in AntPS and PostPS cell populations, respectively (Fig. 1D). Together, our data support that pure populations of AntPS and PostPS cells can be efficiently derived using hPSC-based *in vitro* culture systems.

2.2. Biophysical phenotypes of anterior and posterior primitive streak cells

We next sought to examine biophysical properties of AntPS and PostPS cells derived from hPSCs, including cell morphology, migration behavior, and traction force generation. From phase contrast images recorded at 48 h after differentiation, it was evident that AntPS cells displayed a smaller and spindle cell shape, suggesting a mesenchymal like morphology, whereas PostPS cells had a larger and rounded cell shape, showing an epithelial like morphology (Fig. 2A). Indeed, quantitative data showed that the spread area of AntPS cells was significantly smaller than that of PostPS cells, and the cell shape index of AntPS cells was also significantly less than that of PostPS cells, suggesting a more elongated shape of AntPS cells and a more rounded shape of PostPS cells (Fig. 2B;

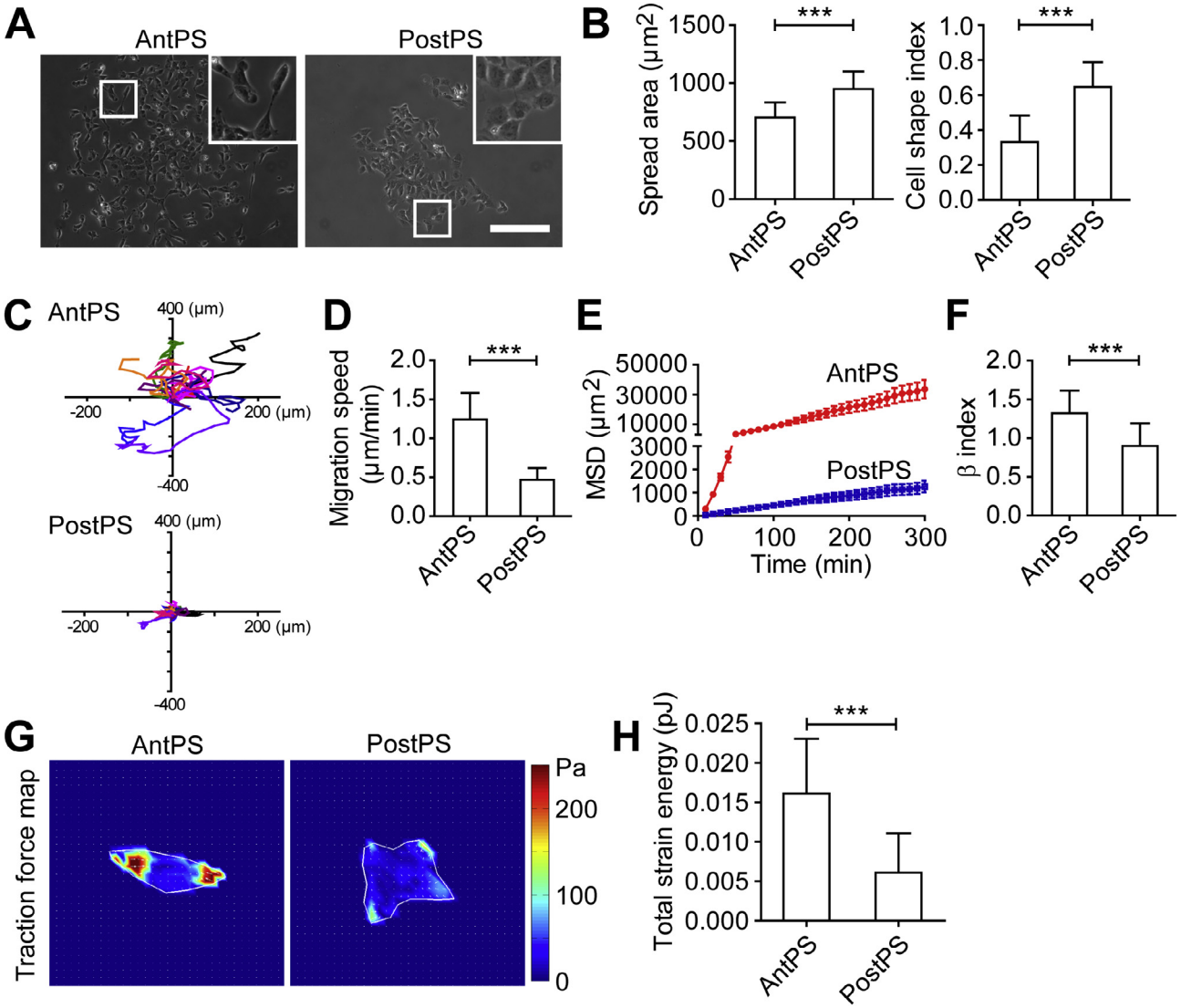

Fig. 2. Anterior and posterior PS cells show different biophysical phenotypes. (A) Representative phase contrast images showing different morphologies between anterior (AntPS) and posterior PS (PostPS) cells. Square inserts show magnified views of cell morphologies. Scale bar, 200 μm. (B) Bar graphs showing quantitative data of cell spread area (left) and cell shape index (right) of AntPS and PostPS cells. Data represent the mean ± SD calculated from at least 150 cells in one experiment that is representative of three independent experiments. (C) Migration trajectories of ten representative AntPS (top) and PostPS (bottom) cells. (D-F) Quantitative data showing migration speed (D), mean square displacement or MSD (E), and migration persistence or β index (F) of AntPS and PostPS cells. Data represent the mean ± SD calculated from at least 50 cells in one experiment that is representative of three independent experiments. (G) Representative traction force maps of individual AntPS and PostPS cells. (H) Bar plot showing total strain energy of individual AntPS and PostPS cells. Data represent the mean ± SD calculated from at least 30 cells in one experiment that is representative of three independent experiments. *P* values were calculated using one-way ANOVA followed by *t*-test analysis. ***, $P < 0.001$.

See Materials and Methods for definition of the cell shape index). Through analyzing migration trajectories of single AntPS and PostPS cells (Fig. 2C), cell migratory behaviors of AntPS and PostPS cells were determined. Migration speed (Fig. 2D), mean square displacement (MSD; Fig. 2E), and migration persistence (β index; Fig. 2F) between AntPS and PostPS cells were distinctly different. AntPS cells displayed faster and more persistent migration than PostPS cells. Measurements of traction force using traction force microscopy (TFM) further revealed that the total strain energy of traction force exerted by single AntPS cell was 2.7-fold higher than that of single PostPS cell. Together, our results demonstrate that AntPS and PostPS cells display significantly different biophysical properties.

2.3. Anterior PS cells have greater migration potential than posterior PS cells in a 3D-like structure

The drastic difference of AntPS and PostPS cells in their biophysical properties further prompted us to examine their migratory behaviors in a more *in vivo*-like 3D environment. To this end, we generated 3D cell spheres containing a mixture of Hoechst-labeled AntPS cells and unlabeled PostPS cells using the hanging-drop method (see Materials and Methods) [19,20]. Migration of AntPS and PostPS cells away from 3D cell spheres was monitored after re-plating cell spheres onto tissue culture dishes (Fig. 3A). Our data revealed that among all cells migrating out of 3D cell spheres, 70 ± 11% were Hoechst-labeled AntPS cells, significantly greater than the percentage of non-labeled PostPS cells (30 ± 11%) (Fig. 3B and Fig. S1). Hoechst labelling has been commonly used in other studies to monitor cell migration [21,22]. Nonetheless, to ensure that Hoechst labelling has a negligible effect on migration of AntPS cells, we also pre-labeled breast cancer cells (MCF7) with Hoechst 33258 before their migratory behaviors were measured in both single cell and 3D sphere assays (the same assays conducted with single AntPS and PostPS cells and 3D cell spheres). There was no significant difference between Hoechst-labeled MCF7 and unlabeled controls as single cells, and the migratory behaviors of labeled and non-labeled MCF7 cells away from 3D cell spheres on 2D surface are not distinguishable (data not shown). Together, our data support that both 2D and 3D cultured AntPS cells have greater migration potential than corresponding PostPS cells on 2D surfaces.

2.4. Anteriorizing and posteriorizing signals regulate biophysical properties of anterior and posterior PS cells

It has been reported that opposite gradients of Activin A and BMP4 along the anterior-posterior axis of the PS, with a greater Activin A activity at the anterior end and a higher BMP activity at the posterior end, play an important role in the formation and pattering of the PS (Fig. 4A) [6,11]. We thus sought to examine whether Activin A and BMP4 signaling could regulate biophysical phenotypes of AntPS and PostPS cells derived from hPSCs. To this end, Activin A and BMP4 concentrations in hPSC differentiation medium were either up- or down-regulated to modulate Activin and BMP activities, respectively (Activin A down: Activin A = 25 ng mL^{-1} and BMP4 = 25 ng mL^{-1}; Activin A up: Activin A = 75 ng mL^{-1} and BMP4 = 25 ng mL^{-1}; BMP4 down: Activin A = 0 ng mL^{-1} and BMP4 = 25 ng mL^{-1}; BMP4 up: Activin A = 0 ng mL^{-1} and BMP4 = 75 ng mL^{-1}; Fig. 4A). hPSCs were treated with these modified differentiation medium for 48 h before being assayed to confirm their AntPS and PostPS cell identifies and determine their biophysical phenotypes. qRT-PCR analyses were conducted to examine expression of AntPS and PostPS cell markers, confirming that hPSCs had indeed undergone anterior and posterior PS differentiation with and without Activin A supplementation in differentiation medium, respectively (Fig. S2). Specifically, mRNA expression levels of AntPS cell markers from both Activin A down and Activin up treatment

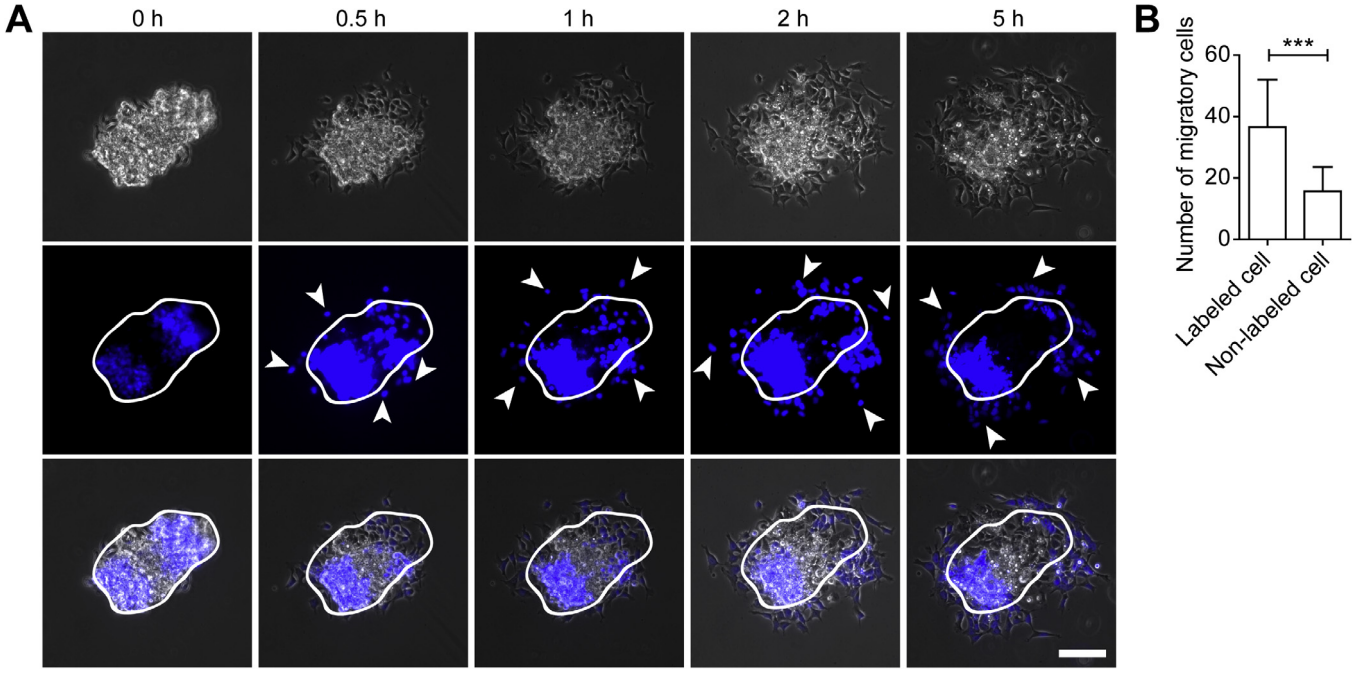

Fig. 3. Anterior PS (AntPS) cells show greater migratory behavior than posterior PS (PostPS) cells in 3D cell clusters. AntPS and PostPS cells were pre-mixed into cell clusters before re-plated onto glass coverslips. AntPS cells were pre-labeled with Hoechst 33258. (A) Representative phase contrast images (top), fluorescence images (middle), and merged images (bottom) showing dissemination of single cells from cell clusters after re-plating for 0, 0.5, 1, 2 and 5 h. White solid lines mark the initial boundary of the cell cluster. White arrowheads mark disseminated individual cells. Scale bar, 200 μm. (B) Bar plot showing the number of AntPS and PostPS cells disseminated from cell clusters 5 h after re-plating. Data represent the mean ± SD calculated from 23 spheres in one experiment that is representative of three independent experiments.

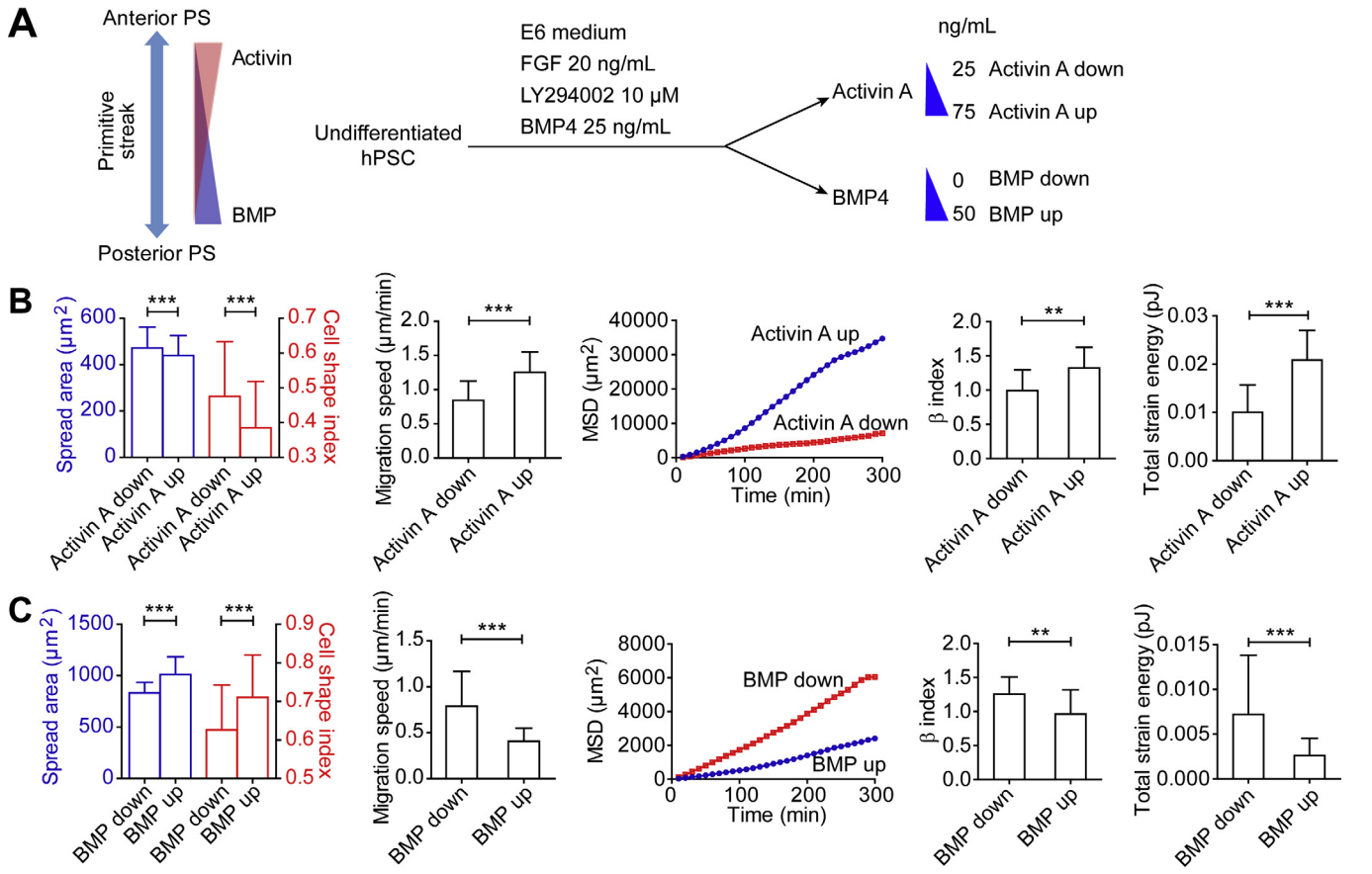

Fig. 4. Effects of anteriorizing *vs.* posteriorizing signaling on biophysical phenotypes of anterior (AntPS) and posterior PS (PostPS) cells. (A) Schematic diagram showing the experimental design of adjusting concentrations of Activin A and BMP4 when deriving anterior (AntPS) and posterior PS (PostPS) cells from hPSCs. (B&C) Biophysical phenotypes of AntPS (B) and PostPS (C) cells as a function of Activin A and BMP4 concentrations, respectively. Data of cell morphology (cell spread area and cell shape index), migration speed, mean square displacement (MSD), migration persistence (β index), and total strain energy are plotted. Data represent the mean ± SD calculated from 150 cells for cell morphology, 50 cells for cell migration, and 30 cells for traction force in one experiment that is representative of three independent experiments. *P* values were calculated using one-way ANOVA followed by *t*-test analysis. **, $P \leq 0.01$; ***, $P \leq 0.001$.

groups were significantly higher than hPSC control group. Similarly, mRNA expression levels of PostPS cell markers from both BMP4 down and BMP4 up treatment groups were significantly higher than hPSC control group.

Our assays to examine the effects of Activin A and BMP4 signaling on biophysical phenotypes of AntPS and PostPS cells revealed that increasing Activin A concentrations from 25 ng mL^{-1} to 75 ng mL^{-1} led to a decrease of both cell spread area (from 471 μm^2 to 439 μm^2) and cell shape index (from 0.47 to 0.38), suggesting a more elongated mesenchymal like morphology (Fig. 4B). Increasing Activin A concentration also resulted in heightened migratory behaviors of AntPS cells, including faster migration speed and greater migration persistence (β index), as well as greater traction force (Fig. 4B). Together, these results suggested that heightened Activin A activity led to a biophysical phenotype more like AntPS cells. In distinct contrast, increasing BMP4 concentrations from 25 ng mL^{-1} to 75 ng mL^{-1} led to a larger and more rounded cell shape, slower migratory speed and less migration persistence, and lower traction force, suggesting a biophysical phenotype more like PostPS cells under heightened BMP signaling (Fig. 4C). Altogether, these data support that Activin A and BMP4 signaling can mediate biophysical phenotypes of AntPS and PostPS cells. Our data are consistent with the notion that Activin A and BMP4 activities serve as anteriorizing and posteriorizing signaling for PS cells, respectively.

2.5. Cytoskeleton contraction mediates anterior and posterior PS cell differentiation

The distinct difference in biophysical phenotypes between AntPS and PostPS cells derived from hPSCs prompted us to examine possible mechanoresponsive molecular mechanism(s) responsible for regulating their differentiation. We thus sought to investigate the role of intracellular cytoskeleton contraction in regulating AntPS and PostPS cell differentiation from hPSCs, as numerous studies have demonstrated the essential role of intracellular cytoskeleton contraction in mediating mechanosensitive stem cell differentiation [13,23]. To this end, we used Y27632 (referred as Y27), a specific inhibitor of ROCK [23], and Blebbistatin (referred as Bleb), a specific inhibitor of the ATPase activity of myosin IIA [24], to inhibit cytoskeleton contraction during AntPS and PostPS cell differentiation of hPSCs. Both Y27 and Bleb have been used in our previous studies as effective inhibitors to block cytoskeleton contractility of hPSCs [23,25].

Under the AntPS cell differentiation condition, inhibition of cytoskeleton contraction through Y27 or Bleb treatments led to an increase of CDX2$^+$ cells from 2.5 ± 1.7% (control) to 21 ± 5.7% or 14 ± 4.2%, respectively, and a decrease of Eomes$^+$ cells from 97.8 ± 1.9% (control) to 79.5 ± 5.3% or 87.5 ± 3.7%, respectively (Fig. 5A). In distinct contrast, under the PostPS cell differentiation condition, abrogation of cytoskeleton contraction through Y27 or

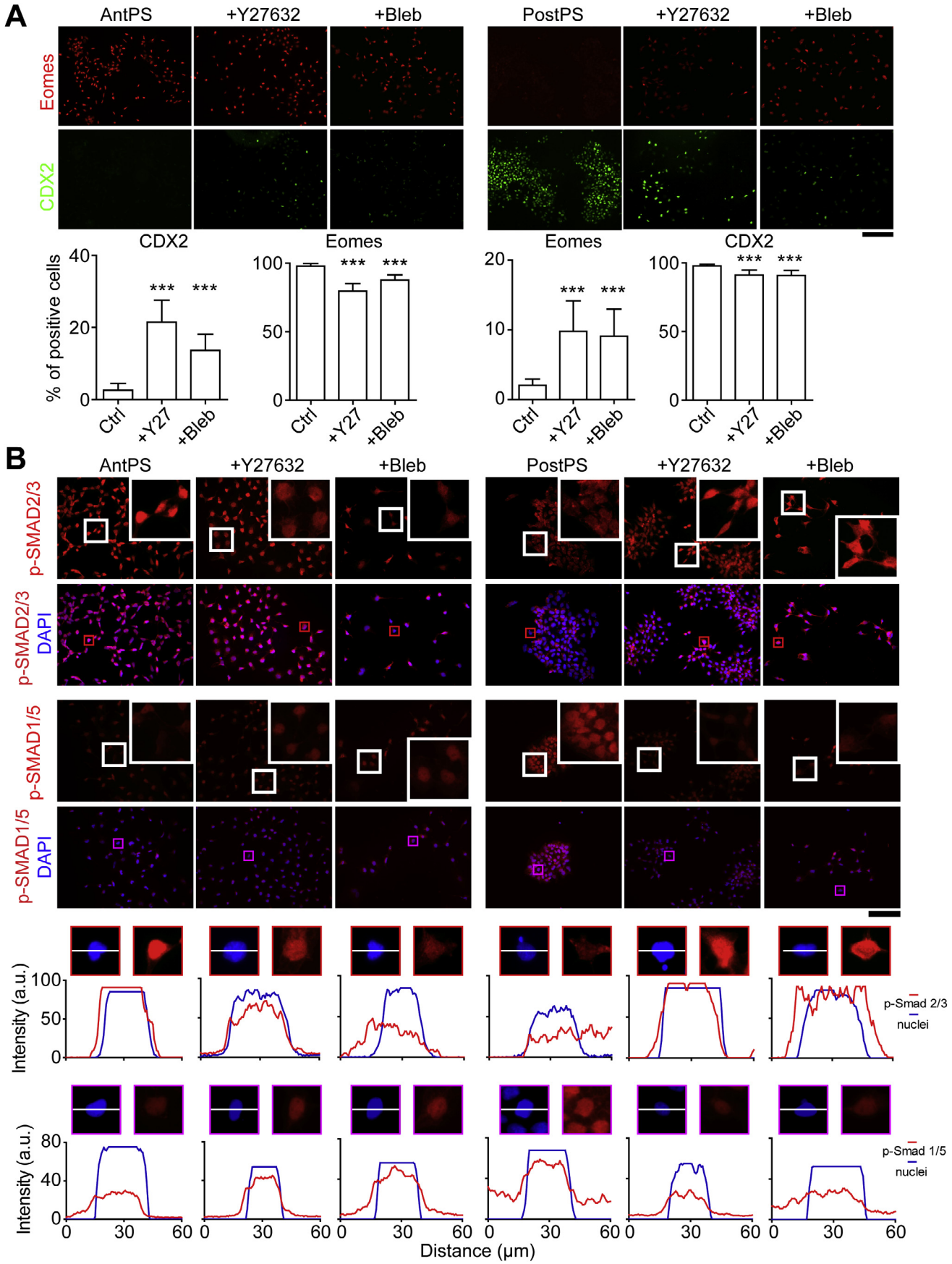
A
AntPS
+Y27632
+Bleb
PostPS
+Y27632
+Bleb
Eomes
CDX2
CDX2
Eomes
Eomes
CDX2
% of positive cells
40
20
0
100
50
0
20
10
0
100
50
0
***
***
***
***
***
***
Ctrl
+Y27
+Bleb
B
AntPS
+Y27632
+Bleb
PostPS
+Y27632
+Bleb
p-SMAD2/3
p-SMAD2/3
DAPI
p-SMAD1/5
p-SMAD1/5
DAPI
Intensity (a.u.)
100
50
0
80
40
0
p-Smad 2/3
nuclei
p-Smad 1/5
nuclei
0
30
60
Distance (μm)

Bleb treatments led to an increase of Eomes$^+$ cells from 2 ± 0.8% (control) to 10 ± 4.1% or 9 ± 3.7%, respectively, and a decrease of CDX2$^+$ cells from 97.8 ± 1% (control) to 91.1 ± 3.5% or 90.8 ± 3.5%, respectively (Fig. 5A). We further examined mRNA expression levels of AntPS and PostPS cell markers in cells treated with Y27 or Bleb. Under AntPS cell differentiation condition, mRNA expression level of AntPS cell markers *Mesp1* and *Eomes* were decreased with Y27 or Bleb treatments, while mRNA expression level of PostPS cell marker *Cdx2* increased with Y27 or Bleb treatments (Fig. S3). Similarly, under PostPS cell differentiation condition, mRNA expression levels of AntPS cell markers *Mesp1*, *FoxA2*, and *Eomes* were upregulated with Y27 or Bleb treatments (Fig. S3).

We further investigated activities of intracellular effectors downstream of Activin A and BMP4 signaling in response to Y27 or Bleb treatments. Activin A and BMP4 are known to activate Smad 2/3 and Smad 1/5 activities through phosphorylation, respectively. Immunostaining assays revealed that almost all AntPS cells showed nuclear staining of p-Smad 2/3, and few cells showed nuclear staining of p-Smad 1/5, whereas almost all PostPS cells had nuclear staining of p-Smad 1/5 but not p-Smad 2/3 (Fig. 5B). Importantly, in AntPS cells, nuclear intensities of p-Smad 2/3 and p-Smad 1/5 as well as percentages of cells with nuclear p-Smad 2/3 and p-Smad 1/5 decreased and increased, respectively, when treated with Y27 or Bleb (Fig. 5B and Fig. S4). In distinct contrast, in PostPS cells, nuclear intensities of p-Smad 2/3 and p-Smad 1/5 as well as percentages of cells with nuclear p-Smad 2/3 and p-Smad 1/5 increased and decreased, respectively, when treated with Y27 or Bleb (Fig. 5B and Fig. S4). Together, these data support that cytoskeleton contraction could regulate intracellular signaling activities downstream of Activin A and BMP4 to mediate PS differentiation and anterior and posterior patterning.

3. Discussion

In this work, AntPS and PostPS cells were successfully derived from *in vitro* hPSC-based culture systems by modulating Activin A and BMP4 supplemented in differentiation medium of hPSCs. Interestingly, AntPS and PostPS cells displayed drastically different biophysical phenotypes, including cell morphology, migration behavior, and traction force generation. Our data support the roles of Activin A and BMP4 in mediating biophysical properties of AntPS and PostPS cells: high Activin A activity leads to more AntPS-like cells, whereas high BMP4 activity results in more PostPS-like cells. This observation is consistent with the common notion that Activin A and BMP4 signaling are essential for mediating AntPS and PostPS cell differentiation from hPSCs, respectively. It has also been well established that *in vivo* there are opposite gradients of Activin A and BMP4 along the anterior-posterior axis of the PS, with a greater Activin A activity at the anterior end and a higher BMP activity at the posterior end. *In vivo*, the PS forms along the caudal midline on the bilaminar embryonic disc [26]. In the early PS stage, embryonic cells in the midline ridge of the epiblast undergo epithelial-to-mesenchymal transition (EMT) and ingress through the PS to first form the definitive endoderm at the anterior end and then the mesoderm at the posterior end [2,4]. AntPS cells are thus precursors of mesoendoderm cells with mesenchymal-like properties, with a smaller cell shape and greater migration properties and traction force generation ability, whereas PostPS cells should have epithelial-like morphology and less prominent migration properties and traction force generation ability. These observations are consistent with our experiment findings.

Cell biophysical phenotypes have been implicated in mediating behaviors and functions of adherent mammalian cells, including both adult and pluripotent stem cells [13,23]. In this work, we demonstrate that cytoskeleton contraction played an important role in mediating AntPS *vs.* PostPS phenotypic switch. Cytoskeleton contraction is known to be mediated by ROCK signaling and the actomyosin cytoskeleton network [27], and our data further supported the roles of ROCK and myosin IIA activities in regulating phenotypic switches between AntPS and PostPS cells derived from hPSCs through their effects on intracellular Smad signaling activities downstream of Activin A and BMP4. Our data are consistent with recent findings of the innate mechanosensitive properties of hPSCs [23,25,28]. Cell contractility has been suggested to play a key role in regulating intracellular signaling events, including Smad signaling, to control gene expression and thus stem cell differentiation [29]. In our previous studies, we have reported that cytoskeletal contractility mediates Hippo/YAP signaling and phosphorylation and nucleocytoplasmic shutting of Smad 2/3 and Smad 1/5 in hPSCs, which act synergistically to control mechanosensitive neuronal differentiation of hPSCs [23]. Our recent work also demonstrates the requirement for BMP-Smad signaling in mechanosensitive amniogenesis of hPSCs [28]. Others have also reported mechanoregulation of BMP signaling through integrins [30] and that integrin-mediated cell contraction regulates TGF β1-Smad signaling [31]. Altogether, these studies strongly suggest an intricate signaling network involving cell adhesion, cytoskeletal contractility and classical developmental signaling (such as TGF-β, BMP and Hippo) to mediate mechanosensitive properties of hPSCs, including AntPS *vs.* PostPS phenotypic switch observed in this work.

Together, we report herein that hPSCs could be used as an *in vitro* model to generate AntPS and PostPS cells that display significantly different biophysical phenotypes. The phenotypic switch of AntPS *vs.* PostPS cells is regulated by Activin A and BMP4 signaling. Importantly, our data further support that cytoskeleton contraction plays an important role in controlling AntPS *vs.* PostPS phenotypic switch through its effect on intracellular Smad signaling activities downstream of Activin A and BMP4.

4. Conclusion

In summary, this study demonstrates that AntPS and PostPS cells display significantly different biophysical phenotypes and reveals an important role of intracellular cytoskeletal contractility in regulating PS differentiation of hPSCs. A detailed role of cytoskeleton contractility in regulating stem cell fate decisions and the molecular mechanism(s) underlying interactions between cytoskeletal contractility and intracellular Smad signaling activities downstream of Activin A and BMP4 remain to be elucidated in the future.

Fig. 5. Intracellular cytoskeleon contraction regulates lineage bifurcation of hPSCs towards anterior (AntPS) and posterior PS (PostPS) cells. (A) Representative immunofluorescence images (up panel) showing Eomes$^+$ AntPS cells and CDX2$^+$ PostPS cells derived from hPSCs under different treatment conditions as indicated. Bar plots (down panel) showing percentages of cells with dominant nuclear staining for Eomes and CDX2 under indicated conditions. Data represent the mean ± SD calculated from at least 10 random fields in one experiment that is representative of three independent experiments. *P* values were calculated using one-way ANOVA followed by *t*-test analysis. ***, $P < 0.001$. Scale bar, 200 μm. (B) Representative immunofluorescence images (up panel) show immunostainning of phosphorylated Smad 2/3 (p-Smad 2/3) and phosphorylated Smad 1/5 (p-Smad 1/5) in AntPS and PostPS cells derived from hPSCs under different treatment conditions as indicated. DAPI counterstains nuclei. White squares show areas where magnified views are included. Red and purple rectangles (down panel) highlight the selected cells, where fluorescence intensities of DAPI, p-Smad 2/3, and p-Smad 1/5 were measured along the white lines drawn across these selected cells. Scale bar, 200 μm. (For interpretation of the references to colour in this figure legend, the reader is referred to the web version of this article.)

5. Materials and methods

5.1. Cell culture

Human pluripotent stem cell (hPSC) line H9 (human embryonic stem cell (hESC), WA09, P50, WiCell; NIH registration number: 0062) was used in the present study. All protocols used for hPSC culture and assays were pre-approved by the Human Pluripotent Stem Cell Research Oversight Committee at the University of Michigan. The H9 hESC line was authenticated as karyotypically normal by Cell Line Genetics (Madison, USA) and was tested negative for mycoplasma contamination (LookOut Mycoplasma PCR Detection Kit, Sigma-Aldrich). The H9 hESC line was cultured on lactate dehydrogenase-elevating virus (LDEV)-free hESC-qualified reduced growth factor basement membrane matrix Geltrex™ (Thermo Fisher Scientific) using a standard feeder-free culture system with mTeSR1 medium (STEMCELL Technologies) per the manufacturer's instruction. The H9 hESC line was used before P70.

5.2. Derivation of primitive streak cells

Anterior and posterior primitive streak (PS) cells were differentiated from hPSCs using protocols previously reported [6,18]. Briefly, hPSCs were digested as single cells using accutase before being seeded onto tissue culture plates or glass coverslips pre-coated with 1% Geltrex solution at 25,000 cells cm^{-2} in mTeSR1 medium containing 10 μM Y27632. On day 1, culture medium was replaced with fresh mTeSR1 medium. On day 2 and 3, cells were treated with anterior and posterior PS differentiation mediums, respectively, with the following compositions: (1) anterior PS differentiation medium: Essential 6™ medium (E6; Thermo Fisher Scientific) supplemented with 20 ng mL^{-1} fibroblast growth factor 2 (FGF2, Peprotech), 10 μM phosphatidylinositol 3-kinase inhibitor (LY294002; Tocris), 25 ng mL^{-1} bone morphogenetic protein 4 (BMP4, R&D Systems), and 50 ng mL^{-1} Activin A (R&D Systems); (2) posterior PS differentiation medium: E6 supplemented with 20 ng mL^{-1} FGF2, 10 μM LY294002, and 50 ng mL^{-1} BMP4. Downstream analyses were performed after cells had been treated with differentiation medium for 48 h. To study effects of different concentrations of Activin A and BMP4 on biophysical phenotypes of anterior and posterior PS cells, we used E6 medium supplemented with 20 ng mL^{-1} FGF2, 10 μM LY294002, and 25 ng mL^{-1} BMP4 as basal medium, together with adding 25 ng mL^{-1} Activin A (referred as Activin A down), 75 ng mL^{-1} Activin A (referred as Activin A up), 0 ng mL^{-1} BMP4 (referred as BMP down), or 25 ng mL^{-1} BMP4 (referred as BMP up).

5.3. Immunostaining

Cells were fixed with 4% paraformaldehyde (Electron Microscopy Sciences) for 30 min at room temperature before being permeabilized with 0.1% SDS for another 30 min at room temperature. Cells were blocked with 2% donkey serum for another 1 h before incubation with primary antibodies (the sources and dilutions were listed in Supplementary Table 1) overnight at 4 °C. Cells were then incubated with Alexa Fluor 488, Alexa Fluor 546, and/or Alexa Fluor 647-labeled donkey-raised secondary antibodies (Invitrogen, 1:400 dilution) for 2 h at room temperature. In addition 4,6-diamidino-2-phenylindole (DAPI, Invitrogen) was used for visualizing cell nuclei. Cells were imaged using an inverted epi-fluorescence microscope (Zeiss Axio Observer Z1, Carl Zeiss Microimaging).

5.4. Analysis of cell morphology and focal adhesion structures

Cell morphology was analyzed by manually tracing cell cytoplasmic borders using the NIH ImageJ software. Shape index (SI) was then calculated as $SI = 2\sqrt{\pi \times cell_area}/cell_perimeter$.

5.5. Migration assay

To examine migratory behaviors of anterior and posterior PS cells, cell migration speed, mean square displacement (MSD), and migration persistence were determined using time-lapse recording of cell positions. In brief, anterior and posterior PS cells were re-plated onto 35-mm glass bottom-tissue culture plates that were pre-coated with 1% Geltrex at a density of 2×10^4 cells per well. After seeding for 6 h, cells were examined under an inverted microscope (Zeiss Axio Observer Z1, Carl Zeiss microImaging) enclosed in an environmental incubator (XL S1 incubator, Carl Zeiss microImaging) maintaining cell culture at 37 °C and 5% CO_2. Cell positions were recorded every 10 min for a total duration of 6 h. Center positions (X/Y coordinates) of each cell was extracted using NIH ImageJ software. Cell migration speed V was calculated as the ratio between cell displacement (D) and time (T) using the following formula [24]:

$$V = \frac{D}{T} = \frac{\sum \sqrt{(X_i - X_{i-1})^2 + (Y_i - Y_{i-1})^2}}{T} \quad (1)$$

where X_i and Y_i were the cell center coordinates at the i-th time point, and T was the total time of cell migration duration. The mean square displacement (MSD) $\left\langle d^2(t) \right\rangle$ was defined as [24]

$$\left\langle d^2(t) \right\rangle = MSD(n\Delta t) = \frac{1}{N-n} \sum_{i=1}^{N-n} \left[(X_{i+n} - X_i)^2 + (Y_{i+n} - Y_i)^2 \right] \quad (2)$$

where Δt was the time interval between two consecutive images, n and N donated the number of time steps and images, respectively. The MSD increases with time as a power-law function [24] as $MSD = D(T/\Delta t)^{\beta}$, and the exponent β is a measure of the migration persistence.

5.6. Traction force assay

To determine traction force generated by PS cells, an improved traction force microscopy (TFM) method was used by anchoring fluorescent beads on surfaces of polyacrylamide (PA) gels [32]. In brief, 35-mm glass bottom dishes were pretreated with bind-silane. PA gels with an acrylamide/Bis- acrylamide ratio of 3%:0.1% (stiffness of 1 kPa) were then prepared and coated onto glass bottom dishes. After polymerization for 30 min at room temperature, PA gel surfaces were coated with 0.5 μm diameter fluorescent beads (rhodamine carboxylate-modified, diluted at 1:50 in water) for 25 min. The beads were covalently linked to gel surfaces by using 1-ethyl-3-[3-dimethylaminopropyl] carbodiimide, hydrochloride (EDC, Invitrogen, 3.8 mg mL^{-1} in 2-(N-Morpholino) ethanesulfonic acid (MES, Sigma), and pH 5.5) and hydroxy-2,5-dioxopyrrolidine -3-sulfonicacid (Sulfo-NHS, Sigma, 7.6 mg mL^{-1} in MES pH 5.5) solution for 2 h and then PBS (pH 7.4) for another 2 h at room temperature [32,33]. The gel substrates were activated by sulfo-SANPAH (Pierce) before functionalized with vitronectin overnight at 4 °C.

Anterior and posterior PS cells were seeded on gel substrates at a density of 2×10^4 cells per well. 6 h after seeding, single anterior and posterior PS cells were imaged in phase contrast. Fluorescence

images of fluorescent beads before and after cell digestion were also imaged. Displacement fields of gel substrates generated by contracting PS cells were calculated using position information of fluorescent beads before and after cell detachment using digital image correlation (DIC) [34]. Cell traction stress fields were then reconstructed by an optimal filtering approach based on the Fourier Transform Traction Cytometry (FTTC) method implemented in MATLAB [35]. To inhibit cytoskeletal contraction, 10 μM Y27632 (referred as Y27) or 10 μM blebbistatin (referred as Bleb) was supplemented into differentiation medium for 48 h during anterior and posterior PS differentiation of hPSCs.

5.7. 3D cell sphere generation

To examine migratory behaviors of anterior and posterior PS cells in a more *in-vivo*-like 3D condition, we generated 3D cell spheres containing a mixture of anterior and posterior PS cells using the hanging-drop method [19,20]. Briefly, per the manufacturer's instruction, anterior PS cells were first pre-labeled with 0.1 mg mL^{-1} Hoechst 33258 for 30 min at 37 °C and 5% CO_2 before being mixed with posterior PS cells at a 1:1 ratio (same cell number) in mTeSR1 medium to achieve a cell density of 1×10^6 cells mL^{-1}. 10 μL cell solution was then placed onto the petri dish cover to generate 3D cell spheres overnight using the hanging drop assay. 3D cell spheres were then re-plated onto 35-mm petri dishes, and cell movements were recorded at 0, 0.5, 1, 2, and 5 h after re-plating to determine the number of migratory cells out of cell spheres.

5.8. Western blotting

Total cell proteins were extracted from cells and separated on SDS-PAGE gels before being transferred to polyvinylidene fluoride (PVDF) membranes. PVDF membranes were incubated with a blocking buffer (Li-Cor) for 1 h at room temperature and then with primary antibodies (the sources and dilutions were listed in Supplementary Table 1) overnight at 4 °C followed by incubation with IRDye secondary antibodies (Li-Cor) for 1 h before protein expression was detected with a Li-Cor Odyssey Sa Infrared Imaging System (Li-Cor).

5.9. RNA isolation and quantitative reverse-transcription PCR (qRT-PCR) analysis

Total RNA was isolated from cells using RNeasy kit (Qiagen) according to the manufacturer's instruction. Reverse transcription of RNA was performed using iScriptTM cDNA kit (Bio-Rad). Quantitative reverse-transcription PCR (qRT-PCR) was performed and monitored using Quantitect SYBR Green MasterMix (Qiagen) and primers (listed in Supplementary Table 2) on a CFX ConnectTM Real-Time system (Bio-Rad) for 40 cycles. Human *GAPDH* was used as an endogenous control for relative quantifications of gene expression by using the $2^{-\Delta\Delta\ Ct}$ method [36]. All analyses were performed with 2–3 biological replicates and 2–3 technical replicates.

5.10. Statistical analysis

For all assays, data were presented as the mean ± standard deviation (SD), unless otherwise noted. Statistical analyses were performed with one-way analysis of variance (ANOVA) followed by *t*-test using GraphPad Prism. A *P* value less than 0.05 was considered as statistically significant.

Acknowledgements

This work is supported in part by the National Science Foundation (CMMI 1129611 and CBET 1149401 to J.F.) and the Department of Mechanical Engineering at the University of Michigan. F. Lin is supported in part by the China Scholarship Council (CSC) Fellowship.

Appendix A. Supplementary data

Supplementary data to this article can be found online at https://doi.org/10.1016/j.actbio.2019.01.017.

References

[1] F.A. Giger, N.B. David, Endodermal germ-layer formation through active actin-driven migration triggered by N-cadherin, Proc. Natl. Acad. Sci. USA (2017). 201708116.
[2] M. Chuai, C.J. Weijer, Who moves whom during primitive streak formation in the chick embryo, HFSP J. 3 (2009) 71–76.
[3] L. Solnica-Krezel, Conserved patterns of cell movements during vertebrate gastrulation, Curr. Biol. 15 (2005) R213–R228.
[4] T. Mikawa, A.M. Poh, K.A. Kelly, Y. Ishii, D.E. Reese, Induction and patterning of the primitive streak, an organizing center of gastrulation in the amniote, Dev. Dynam. 229 (2004) 422–432.
[5] X.J. Lian, X.P. Bao, A. Al-Ahmad, J.L. Liu, Y. Wu, W.T. Dong, K.K. Dunn, E.V. Shusta, S.P. Palecek, Efficient differentiation of human pluripotent stem cells to endothelial progenitors via small-molecule activation of WNT signaling, Stem Cell Rep. 3 (2014) 804–816.
[6] S. Mendjan, V.L. Mascetti, D. Ortmann, M. Ortiz, D.W. Karjosukarso, Y. Ng, T. Moreau, R.A. Pedersen, NANOG and CDX2 pattern distinct subtypes of human mesoderm during exit from pluripotency, Cell Stem Cell 15 (2014) 310–325.
[7] C. Alev, Y.P. Wu, T. Kasukawa, L.M. Jakt, H.R. Ueda, G.J. Sheng, Transcriptomic landscape of the primitive streak, Development 137 (2010) 2863–2874.
[8] S.J. Kattman, A.D. Witty, M. Gagliardi, N.C. Dubois, M. Niapour, A. Hotta, J. Ellis, G. Keller, Stage-specific optimization of activin/nodal and BMP signaling promotes cardiac differentiation of mouse and human pluripotent stem cell lines, Cell Stem Cell 8 (2011) 228–240.
[9] P.F. Xu, N. Houssin, K.F. Ferri-Lagneau, B. Thisse, C. Thisse, Construction of a vertebrate embryo from two opposing morphogen gradients, Science 344 (2014) 87–89.
[10] N.J. Palpant, L. Pabon, C.E. Friedman, M. Roberts, B. Hadland, R.J. Zaunbrecher, I. Bernstein, Y. Zheng, C.E. Murry, Generating high-purity cardiac and endothelial derivatives from patterned mesoderm using human pluripotent stem cells, Nat. Protoc. 12 (2017).
[11] N.J. Palpant, L. Pabon, M. Roberts, B. Hadland, D. Jones, C. Jones, R.T. Moon, W.L. Ruzzo, I. Bernstein, Y. Zheng, C.E. Murry, Inhibition of beta-catenin signaling respecifies anterior-like endothelium into beating human cardiomyocytes, Development 142 (2015) 3198–U3212.
[12] L. Przybyla, J.N. Lakins, V.M. Weaver, Tissue mechanics orchestrate Wnt-dependent human embryonic stem cell differentiation, Cell Stem Cell 19 (2016) 462–475.
[13] A.J. Engler, S. Sen, H.L. Sweeney, D.E. Discher, Matrix elasticity directs stem cell lineage specification, Cell 126 (2006) 677–689.
[14] Y. Sun, C.S. Chen, J. Fu, Forcing stem cells to behave: a biophysical perspective of the cellular microenvironment, in: D.C. Rees (Ed.), Annu. Rev. of Biophys., 2012, pp. 519–542.
[15] SdM. Simoes, A. Mainieri, J.A. Zallen, GTPase and Shroom direct planar polarized actomyosin contractility during convergent extension, J. Cell Biol. 204 (2014) 575–589.
[16] M. Pines, R. Das, S.J. Ellis, A. Morin, S. Czerniecki, L. Yuan, M. Klose, D. Coombs, G. Tanentzapf, Mechanical force regulates integrin turnover in Drosophila in vivo, Nat. Cell Biol. 14 (2012) 935-+.
[17] J.C. Yu, R. Fernandez-Gonzalez, Local mechanical forces promote polarized junctional assembly and axis elongation in Drosophila, Elife 5 (2016).
[18] Y. Shao, K. Taniguchi, R.F. Townshend, T. Miki, D.L. Gumucio, J. Fu, A pluripotent stem cell-based model for post-implantation human amniotic sac development, Nat. Commun. 8 (2017).
[19] O. Frey, P.M. Misun, D.A. Fluri, J.G. Hengstler, A. Hierlemann, Reconfigurable microfluidic hanging drop network for multi-tissue interaction and analysis, Nat. Commun. 5 (2014).
[20] B. Lin, Y. Miao, J. Wang, Z. Fan, L. Du, Y. Su, B. Liu, Z. Hu, M. Xing, Surface tension guided hanging-drop: producing controllable 3D spheroid of high-passaged human dermal papilla cells and forming inductive microtissues for hair-follicle regeneration, ACS Appl. Mater. Interfaces 8 (2016) 5906–5916.
[21] I.Y. Wong, S. Javaid, E.A. Wong, S. Perk, D.A. Haber, M. Toner, D. Irimia, Collective and individual migration following the epithelial-mesenchymal transition, Nat. Mater. 13 (2014) 1063–1071.
[22] J.M. Zahm, H. Kaplan, A.L. Herard, F. Doriot, D. Pierrot, P. Somelette, E. Puchelle, Cell migration and proliferation during the in vitro wound repair of the respiratory epithelium, Cell Motil. Cytoskel. 37 (1997) 33–43.

[23] Y.B. Sun, K.M.A. Yong, L.G. Villa-Diaz, X.L. Zhang, W.Q. Chen, R. Philson, S.N. Weng, H.X. Xu, P.H. Krebsbach, J.P. Fu, Hippo/YAP-mediated rigidity-dependent motor neuron differentiation of human pluripotent stem cells, Nat. Mater. 13 (2014) 599–604.
[24] F. Lin, H. Zhang, J. Huang, C. Xiong, Substrate stiffness coupling TGF-β1 modulates migration and traction force of MDA-MB-231 human breast cancer cells in vitro, ACS Biomater. Sci. Eng. 4 (2018) 1337–1345.
[25] X.F. Xue, Y.B. Sun, A.M. Resto-Irizarry, Y. Yuan, K.M.A. Yong, Y. Zheng, S.N. Weng, Y. Shao, Y.M. Chai, L. Studer, J.P. Fu, Mechanics-guided embryonic patterning of neuroectoderm tissue from human pluripotent stem cells, Nat. Mater. 17 (2018) 633-+.
[26] K.M. Downs, The enigmatic primitive streak: prevailing notions and challenges concerning the body axis of mammals, Bioessays 31 (2009) 892–902.
[27] M. Vicente-Manzanares, X.F. Ma, R.S. Adelstein, A.R. Horwitz, Non-muscle myosin II takes centre stage in cell adhesion and migration, Nat. Rev. Mol. Cell Bio. 10 (2009) 778–790.
[28] Y. Shao, K. Taniguchi, K. Gurdziel, R.F. Townshend, X.F. Xue, K.M.A. Yong, J.M. Sang, J.R. Spence, D.L. Gumucio, J.P. Fu, Self-organized amniogenesis by human pluripotent stem cells in a biomimetic implantation-like niche, Nat. Mater. 16 (2017) 419.
[29] K.H. Vining, D.J. Mooney, Mechanical forces direct stem cell behaviour in development and regeneration, Nat. Rev. Mol. Cell Bio. 18 (2017) 728–742.
[30] J. Du, X.F. Chen, X.D. Liang, G.Y. Zhang, J. Xu, L.R. He, Q.Y. Zhan, X.Q. Feng, S. Chien, C. Yang, Integrin activation and internalization on soft ECM as a mechanism of induction of stem cell differentiation by ECM elasticity, Proc. Natl. Acad. Sci. USA 108 (2011) 9466–9471.
[31] P.J. Wipff, B. Hinz, Integrins and the activation of latent transforming growth factor beta 1 – An intimate relationship, Eur. J. Cell Biol. 87 (2008) 601–615.
[32] K. Liu, Y. Yuan, J. Huang, Q. Wei, M. Pang, C. Xiong, J. Fang, Improved-throughput traction microscopy based on fluorescence micropattern for manual microscopy, Plos One 8 (2013) e70122.
[33] J. Wang, F. Lin, Z. Wan, X. Sun, Y. Lu, J. Huang, F. Wang, Y. Zeng, Y.H. Chen, Y. Shi, W. Zheng, Z. Li, C. Xiong, W. Liu, Profiling the origin, dynamics, and function of traction force in B cell activation, Sci. Signal. 11 (2018).
[34] J.Y. Huang, H. Deng, X.L. Peng, S.S. Li, C.Y. Xiong, J. Fang, Cellular traction force reconstruction based on a self-adaptive filtering scheme, Cell. Mol. Bioeng. 5 (2012) 205–216.
[35] J.Y. Huang, L. Qin, X.L. Peng, T. Zhu, C.Y. Xiong, Y.Y. Zhang, J. Fang, Cellular traction force recovery: An optimal filtering approach in two-dimensional Fourier space, J. Theor. Biol. 259 (2009) 811–819.
[36] K.J. Livak, T.D. Schmittgen, Analysis of relative gene expression data using real-time quantitative PCR and the 2(T)(-Delta Delta C) method, Methods 25 (2001) 402–408.